An empirical potential for interstitial hydrogen in some C-15 Laves phase compounds from IINS measurements

1999 J. Phys.: Condens. Matter 11 10353

(http://iopscience.iop.org/0953-8984/11/50/327)

J. Phys.: Condens. Matter **11** (1999) 10353–10373. Printed in the UK PII: S0953-8984(99)03473-6

An empirical potential for interstitial hydrogen in some C-15 Laves phase compounds from IINS measurements

J F Fernández†§, M Kemali‡, D K Ross‡ and C Sánchez†

† Deparatmento Física de Materiales, Facultad de Ciencias, Universidad Autónoma de Madrid, Cantoblanco 28049, Madrid, Spain

‡ Physics Department, Maxwell Building, University of Salford, Salford M5 4WT, UK

E-mail: josefrancisco.fernandez@uam.es

Received 15 April 1999, in final form 27 September 1999

Abstract. The potential wells seen by hydrogen in several interstitial sites in the C-15 Laves phase compounds, $ZrTi_2$ (ZT), $ZrCr_2$ (ZC) and $TiCr_{1.85}$ (TC), have been investigated using incoherent inelastic neutron scattering (IINS) data. Parameters describing the harmonic terms in the H-potential well in the three compounds are obtained from the first localized hydrogen vibrations as measured by the IINS technique. The H-potential well is created by the sum of the pairwise potentials between the hydrogen and the four metallic atoms forming the different types of tetrahedral site which are labelled g (A_2B_2), e (AB_3) or b (B_4) in the C-15 structure. A Born–Mayer potential has been used to model these pairwise interactions, with parameters determined from the IINS. The resulting overall potential energy surface describes well the observed site occupancies and the diffusional behaviour of H in the ZC and TC compounds. On the other hand, due to the higher H content of the ZT sample, H–H interactions have to be included in the model for a proper description of the energy potential well in this compound. The potential energy surface enables us to identify the different diffusion paths of H in the C-15 structure and hence to infer the different time scales of H diffusion (localized and long-range diffusion) that have recently been shown to exist in these compounds (Skripov A V *et al* 1996 *J. Phys.: Condens. Matter* **8** L319–24; 1997 *J. Alloys Compounds* **253/254** 432–4).

1. Introduction

The behaviour of hydrogen in Laves phase compounds is currently a very active subject of research [1–3], due to hydrogen's high solubility and high diffusivity in these compounds, characteristics that make these systems excellent candidates for use in metal hydride batteries and hydrogen storage applications. In practice, in order to meet the requirements of the applications (high equilibrium pressure and hydrogen solubility and multiple rechargeability), multicomponent alloys of the form $(A_aA_b \ldots A_n)(B_aB_b \ldots B_m)_2$ [4, 5] are used. A large number of compounds with the AB_2 formula crystallize in one of the closely related Laves phases, either the cubic C-15 (ZrV_2, TaV_2) or the hexagonal, C-14 and C-36 ($ZrMn_2$, $ErMn_2$) phases [6, 7], and can accommodate a wide mixture of metals on either the A or B site.

Figure 1 shows the unit cell of the C-15 structure. Three different tetrahedral interstitial sites are available for occupation by H in the phase, namely the g site (A_2B_2), the e site (AB_3) and the b site (B_4). Each unit cell contains 96 g sites, 32 e sites and eight b sites. An example of each of these sites can be seen in the figure. Simultaneous occupation of

§ Corresponding author.

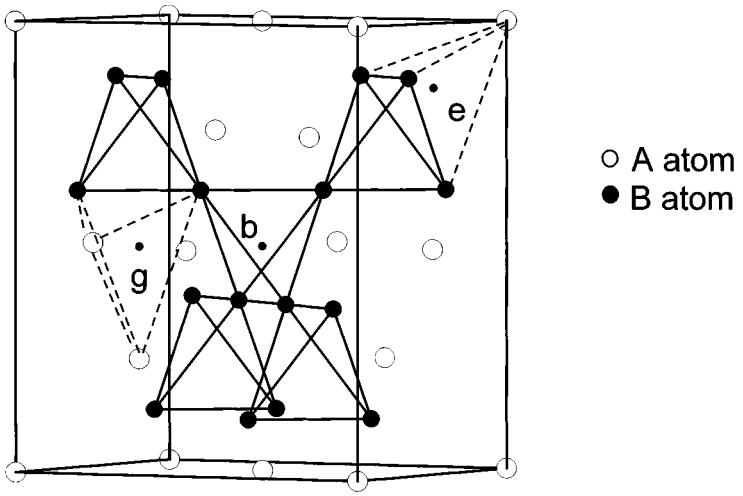

Figure 1. A unit cell of the cubic C-15 structure. The three types of tetrahedral site, g, e and b, are shown in the figure.

all these sites would give a maximum hydrogen to metal ratio, x, of around 6. In practice, significantly smaller concentrations are achievable. Predictions of the site occupied by the H and of the maximum H content in C-15 compounds have usually been made using the so-called Westlake criteria, based on purely geometrical considerations [6]. These criteria state that the radius of the interstitial 'hole', calculated assuming touching hard spheres, should be larger than 0.4 Å and that the distance between hydrogens should be greater than 2.1 Å. Empirical models [8] have also been used in this context. These models aim to predict the heat of formation and the heat of H solution in binary and ternary intermetallics. Application of the Westlake criteria would, in general, lead to the conclusion that, at low H concentrations, the g site is preferentially occupied and that only when the H concentration increases would the e site be partially occupied. Maximum hydrogen to metal ratios of around $x = 2$ are obtained when the above criteria are fulfilled.

IINS (inelastic incoherent neutron scattering) has often been used in the past to investigate metal–hydrogen systems because such measurements yield values of the quanta of vibrational energy associated with motions of the H atom in the metal [9]. The energy gained or lost by the neutron after interacting with the H atom represents the exchange of a quantum of vibrational energy. Energies up to 40 meV are associated with lattice vibrations, the so-called acoustic mode, where the H atom is moving in phase relative to its neighbouring metal atoms. Above 40 meV, typically in the range 50–160 meV, the localized hydrogen vibrations appear. These modes originate, at low concentrations, from the localized hydrogen vibrations at an interstitial site, while for higher concentrations (stoichiometric hydrides) they correspond to propagating optical vibrations where the amplitudes of the metal atoms are negligibly small. For the localized modes, the H can be considered as moving in the potential well formed by its nearest-neighbour metals. One, two or three peaks are observed, depending on the symmetry of the site. The observed number of peaks and their energies yield information on the geometry of the occupied site. Thus, for H in the octahedral sites of an FCC structure (as in Pd) we observe a single peak at around 60 meV [9, 10] and for H in the smaller tetrahedral sites of FCC compounds (Ti, Zr) we also obtain a single peak, but at a higher energy of around 145 meV [10, 11]. On the other hand, two peaks, a singlet and a doublet at 120 and 170 meV, are observed in the α phase of Nb–H, due to the tetragonal distortion of the tetrahedral sites in the

BCC structure [11]. At higher H concentrations, H–H interactions must also be considered. In the stoichiometric case, these interactions can be considered to give rise to dispersion of the optical modes, an effect that has been observed experimentally [12]. Thus, using small amounts of H in a deuteride, it is found that the H vibration is sharp, in contrast to the broad band observed from the corresponding hydride because the deuterons vibrate at a lower frequency and therefore do not couple with the frequencies of isolated H atoms.

At higher energy transfers, successive excited vibrational states are observed in the IINS spectra. If the energy spacings are uniform the potential is close to being harmonic, while if the spacings become more widely spaced the well becomes steeper than harmonic and vice versa. Thus Ikeda *et al* [11, 13] have shown the H-potential wells in Zr and Ti (fluorite structures) are quite close to harmonic while the potentials seen by H in Nb or in V are highly anharmonic. The shape of the H wavefunctions can also be inferred from the Q-dependence of the IINS peak. If the potential is harmonic, the wavefunctions will be given by Hermite polynominals and the Q-dependence of the intensity of the transition from the ground state to the nth excited state will be proportional to $Q^{2n}\exp(-\langle u^2\rangle Q^2)$, where $\langle u^2\rangle$, the m.s.d. of the H in the site, is determined by the parabolic term in the potential. Experimentally, the Q-dependence was shown to be far from harmonic for some of the excited states in $NbH_{0.3}$, although they were harmonic for scattering from the ground state to the first excited states. Using a model potential energy surface, Sugimoto and Fukai [14–16] have performed quantum mechanical calculations on the wavefunctions of the self-trapped state of H in the tetrahedral sites of the BCC metals, V, Nb and Ta. They calculated the energy levels and the wavefunctions of the ground state and the excited states of H by solving Schrödinger's equation for H in the potential well formed by the nearest-neighbour atoms. The pairwise H–metal potentials were modelled by a double Born–Mayer potential containing both a short- and a long-range part. Their results are in agreement with the localized vibrational spectra observed by IINS. The calculated wavefunctions for Nb show the same features as those obtained experimentally [13]. Similarly, Bennington *et al* [17] describe the H potential at the tetrahedral site in the hexagonal α-phase of yttrium by using an anharmonic potential in spherical coordinates. They used perturbation theory to take into account anharmonic effects and H–H interactions. Because, in this system, the H atoms are trapped in pairs either side of an yttrium atom, it was necessary to introduce an H–H interaction to explain the symmetric and asymmetric vibrations of the H pair. More recently, Elsasser *et al* [18] have applied *ab initio* electronic structure calculations combined with the frozen phonon method to obtain the energy surface seen by an H atom in palladium and the excited state energies observed are remarkably close to those observed experimentally [19]. These calculations suggest that the wavefunctions are far from spherically symmetric even in the first excited state and hence that perturbation methods have to be used with great care.

In the absence of first principles calculations, simple Born–Mayer potentials have been used to model H vibrations in metal hydrides. Fukai and Sugimoto [20] have used them to explain the previously observed [10] smooth decrease of the optical mode frequency with lattice parameter in the metal hydrides with the fluorite structure. Stonadge *et al* [21] modelled the potential well of H in the C-15 structure, TaV_2, using fitted Born–Mayer potentials. The parameters of the potential were taken from the observed local mode frequencies in the hydrides TaH_x and VH_x. In a previous publication [22], we have followed a similar approach to analyse the localized modes in the C-15 $ZrTi_2H_{3.6}$.

We present here an IINS study of the hydrogenated C-15 Laves phase compounds $ZrTi_2$ (ZT), $ZrCr_2$ (ZC) and $TiCr_{1.85}$ (TC). We have measured the vibration energies of the local modes of hydrogen in these alloys, and, by using Born–Mayer potentials, have derived parameters to describe the potential well of the hydrogen. In addition to these three compounds, ZT, ZC and TC, we have included in the discussion IINS data on a C-15 $ZrV_2H_{0.5}$ (ZV) compound

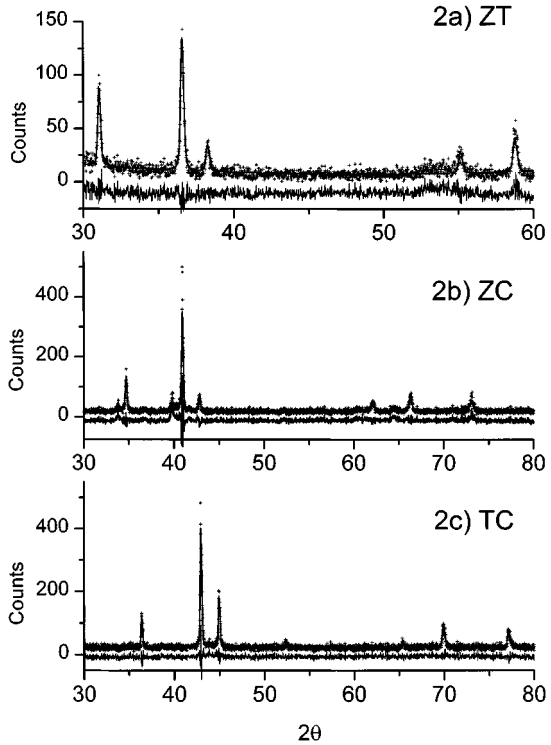

Figure 2. X-ray diffraction patterns at RT from the three samples (a) $ZrTi_2H_{3.6}$ (ZT), (b) $ZrCr_2H_{0.9}$ (ZC) and (c) $TiCr_{1.85}H_{0.4}$ (TC). Solid lines represent the best fit to the data using the Fullprof software. Differences between observed and calculated diffraction patterns are shown at the bottom of each pattern.

measured by other authors [23]. Relative site stabilities and possible diffusion paths can be derived from the resulting potential energy surface.

2. Experiment

The intermetallic alloys were prepared by arc melting the appropriate quantities of the elemental components (99.95% purity) in an argon atmosphere. Several remeltings of the alloys were performed in order to improve their homogeneity. The composition of the samples was checked by energy dispersive x-ray (EDX) analysis. No deviation from the expected compositions were observed. Before hydrogenation, the alloys were annealing at appropriate temperatures (973, 1273 and 1525 K for the ZT, TC and ZC samples respectively) in a vacuum of better than 10^{-3} Pa. This is an important step, particularly for the ZC and TC samples, where both the C-14 and the C-15 phases can be present [24]. Hydrogenation was accomplished in a Sieverts-type apparatus, described elsewhere [25]. The H/metal ratio, x, was determined from the pressure drop in a calibrated volume to an accuracy of 0.01 in x. For the TC sample, surface deactivation with air was needed to prevent loss of hydrogen because of the high equilibrium pressure under ambient conditions [26]. Table 1 shows the values of x for the ZT, ZC and TC samples. Figure 2 shows the x-ray patterns at room temperature for the hydrogenated samples. All of them show the C-15 structure as the main phase. X-ray patterns were refined with the Fullprof software [27] (solid lines in figure 2) and the lattice parameters obtained from

Table 1. Hydrogen to metal ratio, x, lattice parameter at RT, a, local mode energy, E_i, FWHM, Γ_i, and intensity ratio, I_i/I_1, for the three samples, ZT, ZC and TC, at several temperatures, T. The figures in parentheses are the estimated errors in the last digit.

Sample	X (H/Me)	a (Å)	Instrument	T (K)	E_x (meV)	E_y (meV)	E_z (meV)	Γ_x (meV)	Γ_y (meV)	Γ_z (meV)	I_y/I_x	I_z/I_x
ZT	1.2	8.183	TFXA	20	127.5(1)	127.5(1)	169.6(1)	7.8(1)	7.8(1)	8.3(2)	1.00(3)	0.81(3)
				200	127.0(1)	127.0(1)	169.2(2)	8.4(1)	8.4(1)	9.9(3)	1.00(5)	1.17(7)
			IN1B	20	133.6(4)	157.2(4)	143.8(5)	8.7(5)	12.1(5)	9.6(7)	0.80(10)	0.90(20)
ZC	0.3	7.338		190	135.0(7)	161.8(4)	144.4(8)	14.0(5)	15.8(5)	14.2(8)	0.90(10)	0.95(20)
			TFXA	20	132.1(5)	153.3(6)	141.6(5)	7.9(7)	10.3(10)	8.1(10)	0.82(20)	0.90(30)
				20	110.2(2)	160.1(1)	160.1(1)	12.5(3)	12.6(2)	12.6(2)	0.96(4)	0.96(4)
TC	0.13	6.998	IN1B	100	110.5(2)	160.6(1)	160.6(1)	12.5(3)	12.5(2)	12.5(2)	1.07(3)	1.07(3)
				200	110.6(2)	159.7(2)	159.7(2)	14.5(4)	12.2(2)	12.2(2)	1.08(4)	1.08(4)
			TFXA	200	109.7(3)	159.4(2)	159.4(3)	12.6(6)	12.7(3)	12.7(3)	1.05(6)	1.05(6)

the refinement are shown in table 1. The lattice parameters and x-values agree well with the published data on these compounds [26, 28, 29]. The lower intensity for the ZT x-ray pattern is due to an over-large particle size. Even after hydrogenation, this compound is very difficult to crush to an appropriate size for XRD. On the other hand, ZC and TC reduce to a very fine powder during hydrogenation (around 30 μm average diameter). A minority phase was observed for the ZC compound, as can be seen in figure 2. The extra peaks can be indexed as the C-14 phase, which is the stable structure at low temperatures. As mentioned above, the ZC sample was annealed at 1525 K and then quenched to RT to prevent this happening. However, partial transformation to the low temperature C-14 phase was difficult to avoid. On the other hand, the TC and ZT x-ray patterns show no sign of additional phases.

IINS experiments were carried out on both the INIB beryllium filter detector instrument at the ILL (Grenoble, France) (ZC and TC) and the TFXA instrument at the ISIS spallation neutron source (Rutherford Appleton Laboratory, Didcot, UK) (ZT, ZC and TC). TFXA provides a better resolution than INIB, but at a price of a halved counting rate. Spectra were acquired at 20 K and 200 K for the ZC and ZT samples and at 20 K, 100 K and 200 K for the TC sample. The TFXA instrument allows a simultaneous determination of the neutron diffraction pattern at moderate resolution. The diffraction data are very helpful in confirming that there is no phase transformation at the measurement temperatures because this is known to happen below RT in other C-15 alloys, such as ZrV_2 [23] and HfV_2 [30]. The neutron diffraction patterns obtained for the TC and ZT samples correspond to the C-15 structure ($a = 6.97$ Å and $a = 8.16$ Å respectively) in agreement with our x-ray data at room temperature so that the possibility of a phase change can be discarded. For the ZC sample, however, although the C-15 structure is still the main phase ($a = 7.28$ Å), there is evidence of another minority phase which cannot be indexed with the C-14 structure at 20 K. This might suggest that the C-14 phase experiences a phase transition at low temperatures.

3. Results

Figure 3 shows IINS spectra obtained for the three alloys, (a) ZT (TFXA) [22], (b) ZC (IN1B) and (c) TC (IN1B), at several temperatures. The energy axis spans the range from 80 to 220 meV, within which the fundamental modes of the localized hydrogen vibrations (optic modes) appear. Two (ZT), three (ZC) and two (TC) peaks, corresponding to the first H excitations, are observed respectively in the IINS spectra. As can be seen from the figures, additional bands (dashed–dot lines) at 110 meV, 145 meV (ZT), 120 meV, 170 meV (ZC) and 130 meV, 180 meV (TC) appear in the experimental data. These additional bands are too intense to be due to opto-acoustical phonon excitations (side-bands). At the low temperature of the measurements, side-bands on the neutron energy loss side of the main peaks can be expected, but their intensity relative to the fundamental modes, which can be determined by harmonic theory [31], should be only around 0.1–0.15. We believe the additional bands observed in the spectra may be due to hydrogen in other sites in the C-15 structure rather than the regular sites. Also, in the case of the ZC compound, the presence of a minority phase, as observed by x-ray diffraction, may be responsible for these peaks. More discussion will be given below.

Solid lines in figure 3 represent the function fitted to the spectra with three or two bands representing the localized H vibrations plus the additional bands plus the corresponding side-bands (not shown in figure 3) due to opto-acoustic processes (10–15% of the intensity of the local mode). A Gaussian profile is assumed for the optical peaks and also for the side-bands and additional bands. A sloping background has been subtracted from the data prior to fitting. The additional bands in the spectra make it difficult to assign the frequencies. In order to make this assignment in a comprehensive way, in the fitting procedure, we have fixed the

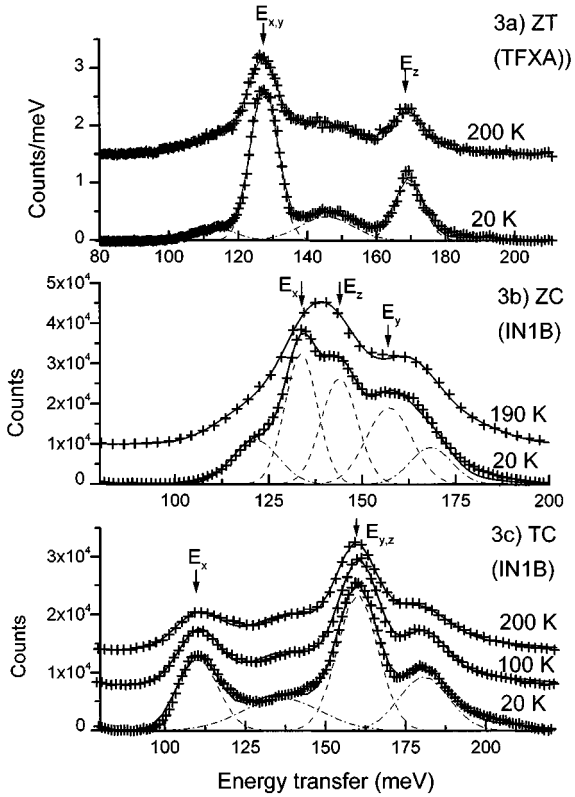

Figure 3. IINS spectra from the three samples (a) $ZrTi_2H_{3.6}$ (ZT), TFXA, (b) $ZrCr_2H_{0.9}$ (ZC), IN1B and (c) $TiCr_{1.85}H_{0.4}$ (TC), IN1B. Spectra at several temperatures are displayed. Solid lines are the best fit to the data with three local modes plus side-bands and additional bands (see text). Local modes and additional bands are shown as dashed and dot–dashed curves respectively. Side-bands are not shown. The mean positions of the local modes at 20 K are shown by arrows.

intensity ratio between the optic modes to be close to 1:1:1 (or 2:1) and have allowed for a small increase of the width of the bands with increasing energy transfer. In doing this, we are assuming that integration over the momentum transfer has little influence on the intensity ratios. As shown in [31], in beryllium filter spectrometers, as is the case for IN1B and TFXA instruments, the relative intensities of the different parts of the one-phonon IINS spectra are, to a first approximation, automatically internormalized for different energy transfers.

The data show that there is no important modification of the spectra with temperature except for the broadening due to reduced lifetimes in the excited states, presumably due to phonon–phonon coupling. Fitting of the high temperature spectra was done starting from the values obtained for the low temperature fit, and allowing for an increase in the width of the peaks and a small change in the intensity ratio due to different Debye–Waller factors. No important change in the position of the peaks was observed with temperature, again indicating that there is no significant change in the structure.

Figure 4 shows TFXA spectra for the ZC (a) and the TC (b) samples obtained from rather short runs. As can be seen from the figure, the statistics are not good enough to improve on the IN1B results for these compounds. The TFXA results are certainly compatible with IN1B spectra and the same optic modes fit both spectra. Table 1 summarizes the parameters

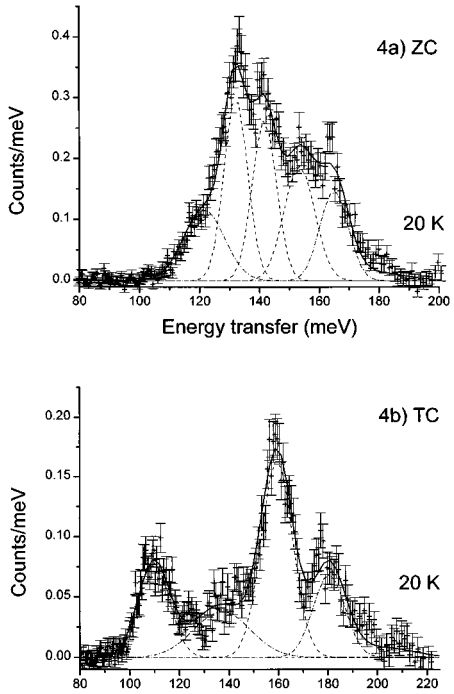

Figure 4. IINS spectra from the ZC and TC samples ((a) $ZrCr_2H_{0.9}$ (ZC) and (b) $TiCr_{1.85}H_{0.4}$ (TC)), from rather short runs at the TFXA instrument. Solid, dashed and dashed–dot lines have the same meaning as in figure 3.

obtained from these fits (fundamental mode energy, E_i, width of the peaks, Γ_i, and the intensity ratio, I_i/I_x, where x refers to the lowest energy mode). As discussed in [22], ZT shows two optical modes, a singlet and a doublet, at 127 and 170 meV respectively (figure 3(a)). This is compatible with H being in an e site which has tetragonal symmetry, as is suggested for this compound by neutron diffraction [29]. Figures 3(b) and 4(a) show the spectra for the ZC sample. These are described in terms of three main peaks at 134, 144 and 157 meV with intensity ratios close to 1. This is consistent with the absence of degeneracy as expected for H in a g site. H occupancy of a g site in ZC is anticipated on the basis of the Westlake criteria and also from fits to the neutron diffraction data [32]. The IINS spectrum obtained for the ZC compound is quite similar to that reported for ZrV_2 [23] at similar H concentrations. The TC sample shows a more complex spectrum (figures 3(c) and 4(b)). Taking into account our criteria of similar intensities for each optical mode, we assign one of these to the 110 meV peak and two overlapping modes to the 160 peak. We therefore need to explain the origin of other peaks in this spectrum, particularly the peak at 180 meV. The $TiCr_{1.85}$ alloy used is clearly non-stoichiometric (we have to use this concentration as the Laves phase structure is not stable at higher Cr/Ti ratios), so that some Ti atoms must occupy B sites, thus forming tetrahedral sites additional to those discussed in the introduction. Figure 5 shows the atomic environment around an A atom in the C-15 structure. There are 12 B atoms surrounding each A atom forming a polyhedron, usually called a Friauf polyhedron. The whole C-15 structure can be built up using these polyhedra. In the TC sample, 7.5% of Cr sites are occupied by Ti. Therefore, about one out of 12 Cr sites in the Friauf polyhedron is occupied by a Ti atom. One Ti on a B site is shared by four g sites. This means that around

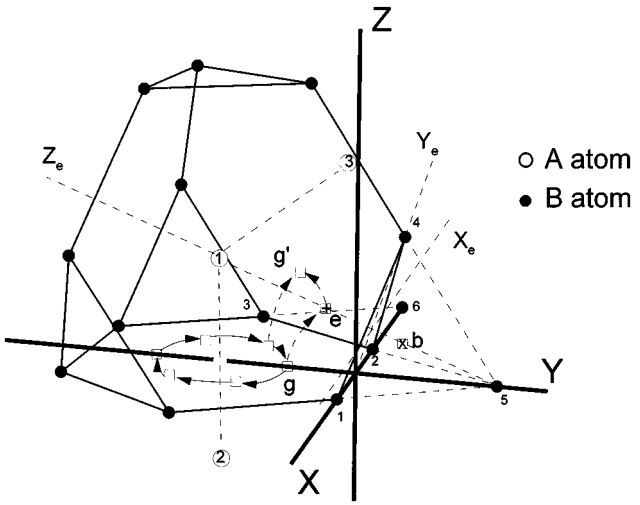

Figure 5. Environment of an A atom in the C-15 structure. The 12 B atoms surrounding the A atom form the so-called Friauf polyhedron. Some of the A and B atoms have been labelled to help the description of sites and planes in the text. Some of the g, e and b sites are shown in the figure. The localized movement of H in a hexagonal ring of the Friauf polyhedron is shown by solid arrows. Long range diffusion takes place across g′ or e sites, dashed arrows.

15% of the normal g sites become 3Ti–1Cr sites. Because of the higher affinity of H for Ti than Cr, we can expect this site to be occupied with a rather higher probability than a normal g site. In addition, around 25% of the e sites become 2Ti–2Cr sites. As shown in the discussion, these two new types of tetrahedral site could explain the new peaks in the spectra.

As mentioned in the introduction, we have included in the discussion IINS data from a C-15 $ZrV_2H_{0.5}$ (ZV) compound measured by other authors [23]. The first localized hydrogen vibrations in this compound appear at energies of 140.4 meV, 146.6 meV and 158.2 meV as measured by IINS at 200 K.

4. The model

For metal–hydrogen systems, motions can be identified on four different time scales: (i) movement of the conduction electrons, (ii) vibrations of the H atoms at high frequency within the almost rigid metal lattice, (iii) H vibrations together with the metal atoms at frequencies of the lattice modes and (iv) diffusive hops of the H atoms between different tetrahedral sites. The movements of electrons are faster than any other motion while hydrogen vibrations are also faster than motions involving movements of the lattice atoms which, in turn, are faster than the diffusive motions of the H atoms, so we assume all these types of motion to be decoupled. Also, the time spent by an H atom on a given lattice site is much longer than the time involved in diffusive jumps between sites. Taking account of these different time scales, we can make use of the Born–Oppenheimer approximation as well as the adiabatic approximation to describe the H as moving in a potential well created by its nearest-neighbour metal atoms. It is assumed that, at each H position, the electronic structure has relaxed to its minimum energy for a particular distribution of positive charges. The shape of the potential well is therefore the variation of total energy of the H–metal system with the displacement of

the H atoms from the centre of the site. The metal atoms will relax adiabatically away from their positions in the absence of H to new positions that minimize the total energy of the system including the energy of the proton in its ground state.

The Hamiltonian for the proton can be written as

$$\left[-\frac{\hbar^2}{2m}\left\{\frac{\partial^2}{\partial x^2}+\frac{\partial^2}{\partial y^2}+\frac{\partial^2}{\partial z^2}\right\}+V(\boldsymbol{r})\right]\varphi(\boldsymbol{r})=E\varphi(\boldsymbol{r}) \tag{1}$$

where $V(\boldsymbol{r})$ is the total potential energy as a function of H position, $\varphi(\boldsymbol{r})$ its wave function and m is the proton mass. As a first approximation, $V(\boldsymbol{r})$ can be considered to be a linear superposition of the potential energies for the interaction of the H with each nearest-neighbour metal atoms. As mentioned in the introduction, H in C-15 compounds occupies only tetrahedral sites, i.e. sites formed by four metal atoms. We have chosen Born–Mayer potentials to describe these interactions. This type of potential was introduced by Born and Mayer [33] to represent the repulsion of closed shell ions in ionic crystals but can equally be used to represent the repulsive core interaction in a metallic system. The attractive part of the metallic interaction due to the conduction electrons is, of course, much more complex, but, as a first approximation, we will neglect it here on the grounds that it will vary slowly with $|\boldsymbol{r}-\boldsymbol{R}_i|$ where $\boldsymbol{R}_i$ is the mean position of the ith neighbouring atom relative to the centre of the site taken as the origin. On this assumption, the total potential energy, $V(\boldsymbol{r})$ is given by

$$V(\boldsymbol{r})=\sum_i C_i \exp\left(-\frac{|\boldsymbol{r}-\boldsymbol{R}_i|}{\rho_i}\right). \tag{2}$$

C_i and ρ_i are parameters characteristic of each metal atom forming the site and the sum is extended to the four nearest neighbour atoms. The eigenvalue problem is solved in the harmonic approximation by expanding the potential to second order around its minimum. By choosing the appropriate Cartesian axes, any second order cross term will disappear (see figure 5 for a description of the Cartesian axes chosen). We are, therefore, left with the eigenvalue problem for a three-dimensional anisotropic harmonic oscillator.

$$V(x,y,z)=V(|r_0|)+\tfrac{1}{2}m\omega_x^2(x-x_0)^2+\tfrac{1}{2}m\omega_y^2(y-y_0)^2+\tfrac{1}{2}m\omega_z^2(z-z_0)^2 \tag{3}$$

where the energy levels are given by the well known formula

$$E=(n_x+\tfrac{1}{2})\hbar\omega_x+(n_y+\tfrac{1}{2})\hbar\omega_y+(n_z+\tfrac{1}{2})\hbar\omega_z+V(|\boldsymbol{r}_0|) \tag{4}$$

where ω_x, ω_y and ω_z are dependent on the C_i and ρ_i parameters and on the $\boldsymbol{R}_i$ distances and are given by

$$\omega_i^2=\frac{1}{m}\frac{\partial^2 V(\boldsymbol{r})}{\partial x_i^2}\bigg|_{r=r_0} \tag{5}$$

where the second derivative is calculated at the minimum of the potential. An extra equation is obtained from the condition for the H atom being at the minimum of the potential. For an H atom in a g site, the first H excitations are given by

$$\hbar\omega_x=\frac{\hbar}{\sqrt{m}}\left[\left(2\frac{C_B}{\rho_B R_B}\left(\frac{d_B^2}{4R_B^2}+\frac{d_B^2}{4\rho_B R_B}-1\right)\exp\left\{-\frac{R_B}{\rho_B}\right\}-2\frac{C_A}{\rho_A R_A}\exp\left\{-\frac{R_A}{\rho_A}\right\}\right)\right]^{1/2} \tag{6a}$$

$$\hbar\omega_y=\frac{\hbar}{\sqrt{m}}\left[\left(2\frac{C_A}{\rho_A R_A}\left(\frac{4R_A^2-d_A^2}{4\rho_A R_A}-\frac{d_A^2}{4R_A}\right)\exp\left\{-\frac{R_A}{\rho_A}\right\}+2\frac{C_B}{\rho_B R_B}\left(\frac{4R_B^2-d_B^2}{4\rho_B R_B}-\frac{d_B^2}{4R_B^2}\right)\exp\left\{-\frac{R_B}{\rho_B}\right\}\right)\right]^{1/2} \tag{6b}$$

$$\hbar\omega_z = \frac{\hbar}{\sqrt{m}}\left[\left(2\frac{C_A}{\rho_A R_A}\left(\frac{d_A^2}{4R_A^2}+\frac{d_A^2}{4\rho_A R_A}-1\right)\exp\left\{-\frac{R_A}{\rho_A}\right\}\right.\right.$$
$$\left.\left.-2\frac{C_B}{\rho_B R_B}\exp\left\{-\frac{R_B}{\rho_B}\right\}\right)\right]^{1/2} \tag{6c}$$

where d_A and d_B are the distances between A and B atoms respectively.

For the case of H in an e site, we obtain

$$\hbar\omega_x = \hbar\omega_y = \frac{\hbar}{\sqrt{m}}\left[\left(\frac{3}{2}\frac{C_B}{\rho_B R_B}\left(\frac{R_B^2-(d-R_A)^2}{\rho_B R_B}-\frac{R_B^2+(d-R_A)^2}{R_B^2}\right)\right.\right.$$
$$\left.\left.\times\exp\left\{-\frac{R_B}{\rho_B}\right\}-\frac{C_A}{\rho_A R_A}\exp\left\{-\frac{R_A}{\rho_A}\right\}\right)\right]^{1/2} \tag{7a}$$

$$\hbar\omega_z = \frac{\hbar}{\sqrt{m}}\left[\left(3\frac{C_B}{\rho_B R_B}\left(\frac{(d-R_A)^2}{\rho_B R_B}+\frac{(d-R_A)^2}{R_B^2}-1\right)\right.\right.$$
$$\left.\left.\times\exp\left\{-\frac{R_B}{\rho_B}\right\}+\frac{C_A}{\rho_A^2}\exp\left\{-\frac{R_A}{\rho_A}\right\}\right)\right]^{1/2} \tag{7b}$$

where d is the distance from the A atom to the basal plane containing the B atoms.

The experimental values for the first hydrogen excitations (table 1) are used as inputs to calculate, through ω_x, ω_y and ω_z, the potential parameters C_A, ρ_A, C_B and ρ_B. The metal–H distances, R_A and R_B, are also obtained by finding the minimum of the potential well.

5. Discussion

For an H atom in a g site, five parameters (C_A, ρ_A, C_B, ρ_B and R_A) have to be fitted in order to fulfil the three equations (6*a–c*) plus the condition of hydrogen being at the minimum of the energy potential. This implies that there is some freedom in the determination of the parameters. This freedom is even higher in the case of a hydrogen atom in an e site where there are only two equations (7*a*, *b*) plus the condition of hydrogen being at the minimum of the energy potential. It would be desirable to obtain a unique set of C–ρ-values that solve the equations. In a previous publication [34] we have shown that this is possible if we solve together the equations for the four compounds, $ZrTi_2$, $ZrCr_2$, $TiCr_{1.85}$ and ZrV_2, under the assumption that the C–ρ-values for each metal, Zr, Ti, Cr or V, are similar in the different compounds. At the same time, we fixed the metal–hydrogen distances, R_A and R_B. For the sake of clarity, we reproduce here the procedure for obtaining the C–ρ-values characteristic of each metal.

The metal–hydrogen distances, R_A and R_B, are fixed in a touching hard-spheres approach by using the values of the hydrogen hole size calculated by Westlake [6] (0.44 Å (ZT), 0.48 Å (ZC), 0.37 Å (TC) and 0.40 Å (ZV) at the H concentrations used in this work) and the well known atomic radii of the metallic elements [6] (1.602 Å, 1.462 Å, 1.282 Å and 1.346 Å for Zr, Ti, Cr and V respectively). These radii are determined on the assumption of close packing in the metal in its elemental form. The calculated values for the metal–hydrogen distances using this approach are summarized in table 2.

To confirm the accuracy of the calculated metal–hydrogen distances we can use neutron diffraction data from Fruchart *et al* [32], Didisheim *et al* [35, 36] and Irodova *et al* [37]. In these works, the position of the deuterium atom in the C-15 ZrV_2D_x, at x values above 1.5, and in the C-15 $ZrCr_2D_x$ compound, at x values higher than 2.89, were studied. To extrapolate their data to the hydrogen content of our samples we can use a result from Didishiem *et al* [35] showing that the coordinates of a D atom in ZrV_2H_x do not vary significantly with deuterium

Table 2. The parameters describing the H-potential well of hydrogen in the four alloys, C_A, C_B, ρ_A and ρ_B. The figures in parentheses are the estimated errors in the last digit; the energy of the local modes, E_i, calculated from these parameters and the metal–hydrogen distances, R_A and R_B, obtained from the hard-sphere approach. The C and ρ values corresponding to the same metal have been marked with the same symbols, ♢ Zr, ● Ti, * Cr and + V. The subscripts A and B stand for the A type atom and B type atom in C-15 AB_2 compound.

Sample	Site	C_A (eV)	ρ_A (Å)	C_B (eV)	ρ_B (Å)	E_x (meV)	E_y (meV)	E_z (meV)	R_A (Å)	R_B (Å)
ZT	e	12 900(150) ♢	0.1800(2) ♢	60 000(600) ●	0.1412(1) ●	127.0	127.0	170.1	2.040	1.904
ZC	g	10 100(80) ♢	0.1800(2) ♢	1 510(13) *	0.1815(2) *	134.8	159.1	143.3	1.990	1.668
ZV	g	10 040(80) ♢	0.1800(1) ♢	10 840(80) +	0.1517(1) +	137.9	161.6	143.4	2.000	1.739
TC	g	51 400(500) ●	0.1403(1) ●	1 350(10) *	0.1784(2) *	109.7	155.2	164.6	1.830	1.666

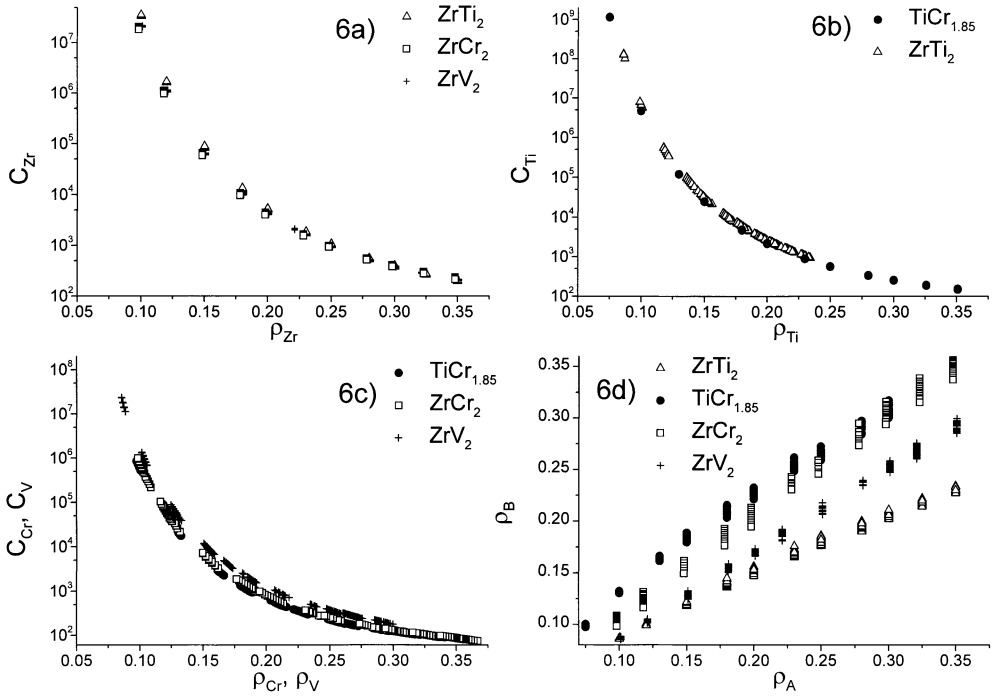

Figure 6. Relationship between ρ (Å) and C (eV) parameters for (a) zirconium in ZT, ZC, ZV alloys, (b) titanium in TC, ZT alloys, (c) chromium and vanadium in ZC, TC and ZV alloys. (d) Relationship between ρ_A and ρ_B in the four alloys. Note the logarithmic scale of the C-axis. See the legend to distinguish between the different symbols. ρ is given in Å and C in eV.

content. Hence, from the change of lattice parameter with deuterium content [32, 35–37] we have calculated Zr–D distances of 1.99 Å and 1.98 Å in $ZrV_2D_{0.5}$ and $ZrCr_2D_{0.9}$, respectively, which are in very good agreement with the values obtained with the hard-sphere method which are shown in table 2, specially taking into consideration the isotopic effect which should increase these distances by around 1%.

Miron *et al* have obtained neutron diffraction data on the deuterated $ZrTi_2D_{3.9}$ C-15 compound [29]. The parameters fitted to these data showed the deuterium to be at the centre of the tetrahedral e site ($R_A = R_B = 1.92$ Å). However, this experiment was done in the early 1970s and it may be that the useful Q-range of the instrument used was not sufficient to resolve a small deviation of the position of the H from the centre of the e site, as we would predict in these four compounds. Deviations from the centre of the site as predicted here have, in fact, been observed in the similar C-15 systems $ZrCr_2D_x$ [32, 37], ZrV_2D_x [35, 36] and TaV_2D_x [38] ($x > 1$).

We have studied the solutions of equations (6*a–c*) by a trial and error method and the results can be seen in figures 6(a)–(d). The x-axis spans the ρ-range in which it is possible to find solutions to equations (6*a–c*) for the imposed metal–hydrogen distances. The variation of C with ρ for Zr (a), Ti (b) and Cr and V (c) in the four compounds ZT, ZC, TC and ZV are shown. To obtain these curves we allow for a small variation of the metal–hydrogen distances of 0.001 Å from the value calculated with the touching hard-spheres method and also we have taken into account the error involved in the determination of the experimental frequencies, 1 meV for isolated peaks and 2–5 meV in the case of overlapping peaks.

These uncertainties give rise to a range of C–ρ-values that solve the equations as can be seen in figures 6(a)–(c).

The second condition we have to apply to arrive at a unique set of C_{Zr}, ρ_{Zr}, C_{Ti}, ρ_{Ti}, C_{Cr}, ρ_{Cr}, C_v and ρ_v values is to assume that the parameters of the potential created by each metal in the different alloys are similar. As can be seen from figure 6(a), the C–ρ-curves for Zr in the different compounds are quite similar. This means that if we assume similar ρ_{Zr} values in ZT, ZC and ZV compounds then the C_{Zr} values are also similar and then the interatomic potential created by zirconium in the three compounds is similar. This conclusion can also be extended to the titanium atom in ZT and TC compounds (figure 6(b)) and to the chromium atom in ZC and TC compounds (figure 6(c)). However, the assumption that the same ρ_{Zr} value holds for Zr in ZT, ZC and ZV compounds, the same ρ_{Ti} holds for Ti in TC and ZT compounds and the same ρ_{Cr} holds for Cr in TC and ZC compounds put some restrictions on the possible ρ values. This can be seen in figure 6(d) where the dependence of ρ_B on ρ_A in the four alloys is shown. An almost linear dependence is obtained. If we chose a certain value for ρ_{Zr} in the ZT alloy, let us say 0.15 Å , the value for ρ_{Ti} should be around 0.12 Å. Then ρ_{Ti} in the TC alloy should be also around 0.12 Å which fixes the possible ρ_{Cr}-values in the TC and ZC alloys. A best fit is obtained when ρ_{Zr} in ZT is as close as possible to its value in ZC and ZV, ρ_{Ti} in ZT is as close as possible to its value in TC and ρ_{Cr} in ZC is as close as possible to its value in TC. Once the ρ-values have been fixed for each metal, the C-values can be directly obtained from figures 6(a)–(c).

Table 2 shows the parameters obtained from the analysis above to describe the energy potential well of H in the ZT, ZC, TC and ZV compounds. The values quoted in table 2 are those showing the smallest differences for the same metal in the different alloys. As can be seen, the potential well can be described by C- and ρ-parameters characteristic of each metal, with small variations between them. The first excited state energy level differences calculated from the fitted C- and ρ-values are also given in table 2 for the preferred sites in each compound. These values can be compared with the experimental values recorded in table 1. As can be seen, good agreement is obtained. In the following, we will use these C–ρ-values to discuss the site occupancy and diffusion behaviour of hydrogen in the four compounds.

5.1. Relative stability of the H sites

For the TC, ZC and ZV samples, where the H is in a g site, the x-, y- and z-directions are as shown in figure 5. Thus the three vibrations, ω_x, ω_y and ω_z correspond respectively to vibrations parallel to a line joining adjacent B atoms which is perpendicular to a line joining A atoms, a vibration perpendicular to the lines joining adjacent A and adjacent B atoms and a vibration parallel to adjacent A atoms which is perpendicular to adjacent B atoms. For H in the e site of the ZT sample, the axes are shown in figure 5 as X_e, Y_e and Z_e. The frequencies ω_x, ω_y correspond to vibrations in a plane parallel to the X_e–Y_e-plane containing the B atoms and ω_z is a vibration along the Z_e-axis. Figure 7 shows a comparison between the Born–Mayer potential (solid lines) calculated from the C- and ρ-values given in table 2 and the harmonic approximation (dot–dashed lines) used to calculate first excited state energies along the three directions, X, Y and Z. Figures 7(a)–(c), (d)–(f) and (g)–(i) correspond respectively to the ZT (e site), ZC (g site) and TC samples (g site). As can be seen, the harmonic approximation holds, approximately, for the ZC and TC compounds but it is not as good for the Y- and Z-directions of the ZT compound (e site). This departure from harmonic behaviour is expected from the asymmetry of the e site in that direction. The ground state and first excited state are also shown in the figure for all cases. It should be noted that the ground state and first excited state lie close to the harmonic range of the potential, except for the Y- and Z-directions in the ZT sample where they are clearly in the anharmonic region.

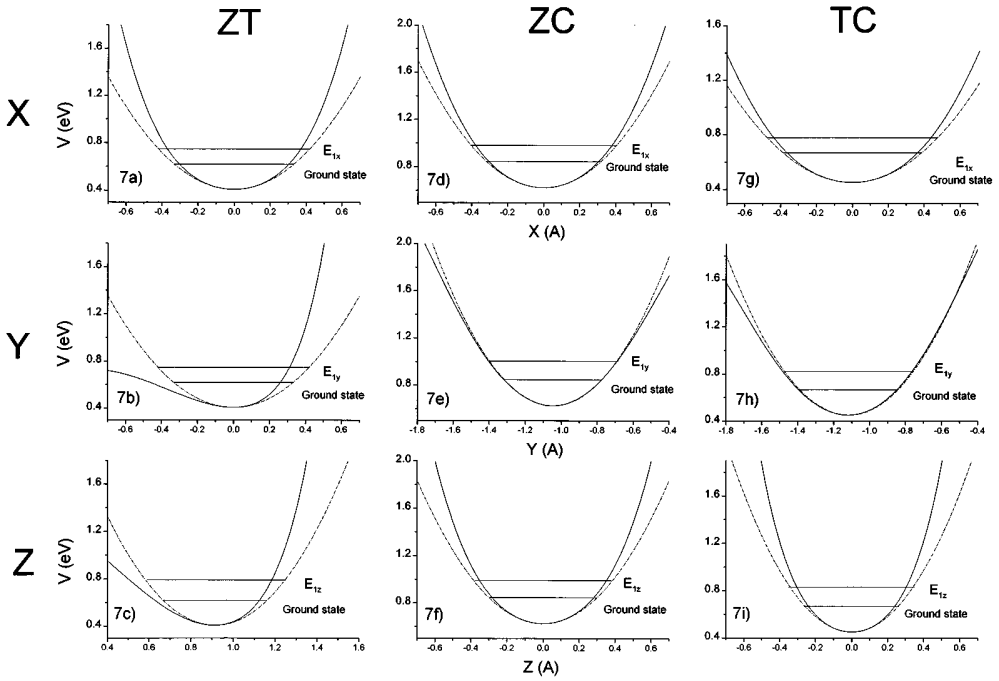

Figure 7. Comparison between Born–Mayer potential (solid lines) and its harmonic approximation (dashed–dot lines) along the three directions, X, Y and Z (X_e, Y_e and Z_e for ZT) for the three compounds, ZT (a)–(c), ZC (d)–(f) and TC (g)–(i). The ground state and the first excited states are also shown. Distances along the axes are given in Å.

Figure 8 shows a contour map plot of the H energy potential in the XY- and YZ-planes for the three compounds TC (a), (b), ZC (c), (d) and ZT (e), (f). Contour lines are plotted every 0.05 eV. In constructing the energy potential surface, we have taken into account atoms A_1, A_2, B_1, B_2 and B_3 for the XY-plane and atoms A_1, A_2, B_1, B_2, B_4 and B_5 for the ZY-plane (see figure 5). Two minima are shown in the XY-plane. These correspond to two of the six g sites lying at a face of the Friauf polyhedron. The saddle point between these sites can also be observed in the figure. The three tetrahedral sites g, e and b as well as the saddle points between them are shown in the ZY-plane in figures 8(b), (d), (f).

Figure 9 shows a contour map plot of the H-energy-potential well in a plane containing the A atoms labelled 1, 2 and 3 in figure 5. This plane is perpendicular to the XY-plane and forms a 60° angle to the ZY-plane. The separation between contour lines is 0.05 eV and the atoms used to generate the potential are A_1, A_2, A_3, B_2, B_3 and B_6 . In this plane three potential minima are observed, corresponding to two g sites on different faces of the Friauf polyhedron (labelled g and g′) and to an e site. Although the energy potentials around the g, g′ and e sites are identical to those shown in figure 8, the saddle point between g and g′ sites is different to that between g and g′ sites as discussed below.

Values of the calculated energy potential at the different minima V_g, V_e and V_b and at the saddle points V_{g-g}, V_{g-e}, V_{e-b} and $V_{g-g'}$ are collected in table 3. The relative stability of each site is given by this potential energy plus the sum of the those zero point energies at the site. In the harmonic approximation, the zero point energy is given by $\sum \hbar\omega_i/2$ while the extra energy at the saddle points is obtained similarly from the two perpendicular potential energy curvatures at the saddle. Table 3 shows the zero point energies, E_0, at g and e sites and at

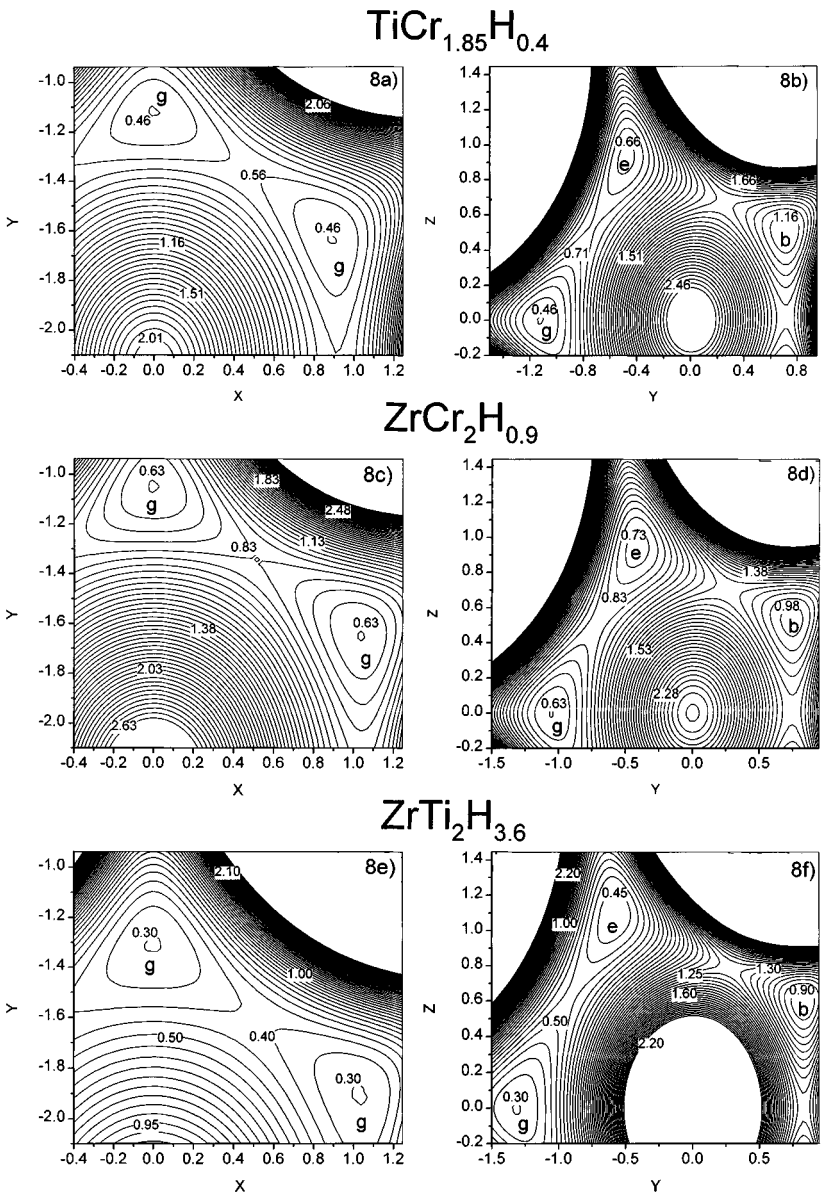

Figure 8. Contour plots of the hydrogen energy potential for the three compounds, TC (a), (b), ZC (c), (d) and ZT (e), (f), in the XY-plane (a), (c) and (e) and in the YZ-plane (b), (d) and (f). Contour lines are drawn every 0.05 eV. See figure 5 for a definition of the axes. The potential energy value at several representative contour lines is shown. Distances along the axes are given in Å.

the saddle points between the g–g sites, g–e sites and g–g′ sites, calculated from the energy potential surface in the harmonic approximation. According to our results, the g site is the most stable site in all four compounds ($V_g + E_{0g}$). As expected from its small size, the b site is always far away in energy from the other two, indicating that this site should always be empty. Assuming a Boltzmann distribution for the occupation of the sites, the differences in energy between the g and e sites implies that only the g site is occupied at temperatures below RT.

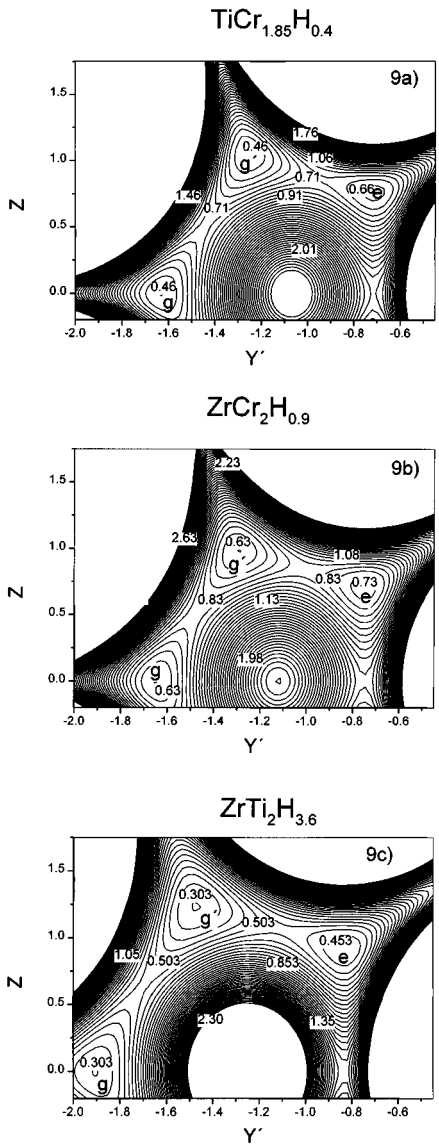

Figure 9. Contour plots of the hydrogen energy potential for the three compounds in a plane perpendicular to the XY-plane and form a 60° angle to the ZY-plane, TC (a), ZC (b) and ZT (c). Contour lines are drawn every 0.05 eV. The potential energy value at several representative contour lines is shown. Distances along the axes are given in Å.

Neutron diffraction on $ZrCr_2D_x$ ($x > 2.89$) [32] and ZrV_2D_x ($x > 1.5$) [35, 36] shows that only the g sites are occupied at low D concentration and only a fraction of e sites are occupied at the maximum D content. Also, from [6] it is concluded that, for TC, ZC and ZV samples, the g site should be the stable one. On the other hand, to calculate the potential parameters for the ZT compound, we have assumed that H occupies the e site, as has been shown before from neutron diffraction data [29]. This is in contrast to the fact that the energy potential is smaller at the g site. We attribute this anomaly to the high H content of this sample which contains

Table 3. Values of the potential at g, V_g, e, V_e, and b, V_b, sites as well as at the saddle points between g sites sharing the same hexagonal face in the Friauf polyhedron, V_{g-g}, g and e sites, V_{g-e}, g and g′ sites at different hexagonal faces of the Friauf polyhedron, $V_{g-g'}$, and e and b sites, V_{e-b}. The zero point energy, E_0, at g and e sites and at g–g, g–e and g–g′ saddle points is also included.

Sample	V_g	E_{0g}	V_e	E_{0e}	V_b	V_{g-g}	E_{0g-g}	V_{g-e}	E_{0g-e}	V_{g-g}	$E_{0g-g'}$	V_{e-b}
ZT	0.302	0.174	0.409	0.212	0.858	0.405	0.174	0.545	0.218	0.545	0.208	1.325
ZC	0.630	0.219	0.705	0.228	0.955	0.830	0.218	0.855	0.219	0.855	0.203	1.195
ZV	0.531	0.221	0.624	0.248	0.982	0.715	0.217	0.805	0.244	0.805	0.230	1.365
TC	0.456	0.215	0.639	0.235	1.109	0.565	0.233	0.755	0.219	0.745	0.196	1.365

3.6 H atoms for every Zr atom; i.e. 3.6 out of the 12 g sites in the tetrahedron should be filled. This cannot be done without violating the Westlake criteria, which state that the minimum distance between H atoms is 2.1 Å. On the other hand, the occupation of a proportion of e sites by H allows us to fulfil both criteria, namely the distance between H atoms and the size of the hole [6]. To represent the repulsive potential between H atoms, we assume a linearized Thomas–Fermi approximation [39]. In this scheme, an interstitial proton attracts some valence electrons to screen the positive charge. In the linearized approximation the interaction between the H atoms assume the form

$$V_H(r) = (e^2/4\pi\varepsilon_0)\frac{\exp(-k_0 r)}{r}$$

where k_0^{-1} is the screening radius, which can be calculated in the free electron approximation, e is the electron charge and ε_0 is the dielectric constant of vacuum. We have calculated a k_0^{-1} value of 1.99 Å for an electronic density of 15.2×10^{22} cm^{-3} for the $ZrTi_2H_{3.6}$ compound. Assuming that H is in the e site, and taking into account the distances between nearest neighbour pairs of g and e sites ($d_{e-g} = 1.30$ Å and $d_{e-e} = 2.45$ Å [6]), the potential energy at the g site and e site become $V_g = 1.13$ eV and $V_e = 0.44$ eV respectively. These values clearly show that H–H interactions make the e site lower in energy than the g site. Therefore, for this compound, with a high H content, H–H interactions have to be included in the calculations. This is not the case for the ZC, ZV and TC compounds because the low H concentration makes it possible to have H on g sites far enough away from each other.

The model also allows us to predict the expected energy level differences for H in the possible alternative tetrahedral sites in the C-15 structure. These energies have been calculated for the e sites in the ZC, TC and ZV compounds and for the g site in the ZT compound. The energies for the e sites in the ZC, TC and ZV samples are higher (138 meV (doublet), 180 meV (singlet) for ZC, 129 meV (doublet), 211 meV (singlet) for TC and 151 meV (doublet), 194 meV (singlet) for ZV) than those obtained for the g sites, reflecting the smaller size of the e sites in these compounds. In the case of H in the g site of the ZT compound, however, we predict energies of 104 meV, 117 meV and 127 meV for the three modes of vibration. The additional weak peak at 110 meV observed in the IINS spectrum of the ZT sample, figure 3(a), could be an indication of partial occupancy of the g site in this compound although the above mentioned inaccuracy of the energy potential well for this compound mentioned above should be remembered.

As mentioned in the results section, the additional peaks observed in the TC spectra (figures 3(c) and 4(b)) could be due to vibrations of H in g or e sites where a Cr atom has been replaced by a Ti atom. We have calculated local mode energies of 102 meV, 177 meV and 201 meV for a 3Ti–1Cr g-type site and local mode energies of 129 meV, 130 meV and 193 meV for a 2Ti–2Cr e-type site, ignoring any atomic displacements. These values should

be considered just as a rough approximation as we have not included the site relaxation due to the replacement of a Cr atom by a Ti atom which should reduce the local mode energies. Anyway, the local mode energies for the 2Ti–2Cr e-type site are similar to those of the additional peaks observed in figure 3(c), 130 meV and 180 meV. Thus it is reasonable to suggest that the additional peaks in the IINS spectra of the TC sample are due to the localized hydrogen vibrations in this site.

5.2. The activation energy for H diffusion

In the temperature range in which over-barrier jumps become important, activation energies for the diffusion of H can also be estimated from our energy potentials. Diffusion of interstitials by thermal activation has been calculated before by Vineyard [40] on the basis of classical absolute rate theory. Later Katz *et al* [41] and Le Claire [42] introduced quantum corrections and anharmonic effects to Vineyard's formulae. Assuming that the lattice modes are not very different at the bottom of the potential and at the saddle points, we can arrive at an expression for the activation energy, given by

$$E_a = V_s - V_0 - \frac{1}{2}\sum_{i=1}^{3}\overline{h}\omega_{i0} + \frac{1}{2}\sum_{i=1}^{2}\overline{h}\omega_{is}$$

where V_s and V_0 are the energies at the saddle point and at the bottom of the potential respectively and the third and fourth terms are the zero point energy at the bottom of the potential and at the saddle point respectively. Zero point energy values are shown in table 3. Energies between 0.20 eV and 0.25 eV were obtained for the g–g, g–e and g–g′ saddle points. (We have not included the ZT compound in our discussion of activation energies as we have shown above that H–H has to be included in the calculation of the energy potential well for this compound at this H concentration.)

Table 4. Activation energy obtained from our calculations for H jumping between g sites in the same hexagonal face of the Friauf polyhedron, E_a(g–g), between g and e sites, E_a(g–e) and between g sites in different hexagonal faces of the Friauf polyhedron, E_a(g–g′).

Sample	E_a(g–g) (eV)	E_a(g–e) (eV)	E_a(g–g′) (eV)
ZC	0.20	0.23	0.21
ZV	0.18	0.30	0.28
TC	0.13	0.30	0.27

Table 4 shows the resulting activation energy between g sites, E_{g-g}, g–e sites, E_{g-e}, and g–g′ sites, $E_{g-g'}$, for ZC, ZV and TC compounds. The most interesting feature of these values is that smaller activation energies are obtained for the g–g path as compared to g–e path and g–g′ path. It should be realized that H jumps between g and g sites represents a localized motion as H cannot escape from the hexagonal face of the Friauf polyhedron by this mechanism. In figure 5 this localized movement in an hexagonal ring is shown by arrows. In order to move to another polyhedron, H atoms have to jump across to a g′ site or go via an e site. Therefore the differences in E_a could be related to two different mechanisms of diffusion, localized diffusion between g sites, and long range diffusion via g–e or g–g′ jumps.

It is interesting to note that activation energies in the range of 0.2 eV have been obtained [43] for long range diffusion in several C-15 Laves phase compounds. Experimental evidence of localized motion has also been reported by several authors [1–3, 44]. Bowman *et al* [44] have measured the proton relaxation time in $TiCr_{1.85}H_x$ in the low (α-phase) and

intermediate (α'-phase) for H contents in both the C-15 and C-14 structures. For a C-15 $TiCr_{1.85}H_{0.55}$ sample they obtained large differences in E_a above and below 180 K. They interpreted their results as being due to two different mechanisms of diffusion, a localized motion with an E_a value of 0.03 eV and long range diffusion with an E_a of 0.19 eV. This is in agreement with results obtained from out model although we have obtained rather larger E_a values. Renz *et al* [45] have studied the H mobility in C-14 and C-15 $ZrCr_2H_x$ samples by pulse field gradient nuclear magnetic resonance. They observed marked deviations from Arrhenius behaviour in the hydrogen diffusivity at low temperatures down to 180 K. The E_a for long range diffusion obtained from the high temperature part of their data is 0.146 eV, which is also smaller than the value obtained by us for g–g′ and g–e jumps.

Our results suggest that two different mechanisms of H motion in C-15 Laves phase compounds are possible: a fast localized motion with an activation energy between 0.1 eV and 0.2 eV, corresponding to jumps between g sites placed on the same hexagonal faces of the Friauf polyhedron. The second mechanism is the long range diffusion via jumps between g–e sites of g–g′ sites with an activation energy higher than 0.2 eV.

6. Conclusions

IINS spectra of the C-15 Laves phase compounds $ZrTi_2H_{3.6}$, $ZrCr_2H_{0.9}$ and $TiCr_{1.85}H_{0.4}$ have been acquired at temperatures between 20 K and 200 K and the local modes of hydrogen in these alloys have been measured. The IINS spectrum of the ZT sample is composed of a doublet at 127.5 meV and a singlet at 169.6 meV. For the ZC sample we have obtained three optic modes at 133.6 meV, 143.8 meV and 157.2 meV. Finally, a peak at 110.2 meV and two overlapped peaks at 160.1 meV have been measured for the TC sample. This information has been used to derive the energy potential well seen by H atoms in these alloys. The energy potential has been built up using interatomic potentials of the Born–Mayer type for each of the metal atoms forming the tetrahedral sites, g (A_2B_2), e (AB_3) or b (B_4). The calculated potentials provide a good description of the observed site occupancies and of the diffusion behaviour of H in the ZC, TC and ZV (IINS data from [23]) compounds. On the other hand, due to the higher H content of the ZT sample, H–H interactions have to be taken into account for a proper description of the potential energy surface in this compound. The energy potential allows us to infer the different diffusion paths of H in the C-15 structure. It has been shown that the activation energy for diffusion of hydrogen between g sites sharing the same face of a Friauf polyhedron (g–g jumps) is smaller than the E_a values for jumps between g sites on different faces of the Friauf polyhedron (g–g′), or from g to e sites. This can be related to the different time scale motion (localized and long range diffusion) of the H atoms that have been shown recently to exist in Laves phase compounds.

The empirical potential model we have developed is not perfect but it is a reasonable starting point for modelling other aspects of the system and is probably as good as possible until first principles ‘frozen phonon’ type calculations become available.

Acknowledgments

We thank the Spanish/British Integrated Actions (HB1996-0041) for partial support and the ILL and the Rutherford Appleton Laboratory for providing the neutron scattering facilities. Two of us (JFF and CS) also thank the Spanish DGICYT (PB96-0084).

References

[1] Skripov A V, Cook J C, Karmonik C and Hempelmann R 1996 *J. Phys.: Condens. Matter* **8** L319–24
[2] Skripov A V, Cook J C, Karmonik C and Hempelmann R 1997 *J. Alloys Compounds* **253/254** 432–4
[3] Skripov A V, Cook J C, Sibirtsev D S, Karmonik C and Hempelmann R 1996 *J. Phys.: Condens. Matter* **8** L319–24
[4] Percheron-Guegan A and Welter J M 1992 *Hydrogen in Intermetallic Compounds* vol I, ed L Schlapbach (Berlin: Springer) pp 11–48
[5] Hempelmann D, Richter D, Pugliesi R and Vinhas L A 1983 *J. Phys. F: Met. Phys.* **13** 59–68
[6] Westlake D G 1983 *J. Alloys Compounds* **90** 251–73
[7] Yartis V A, Burnasheva V V and Semenenko K N 1983 *Russ. Chem. Rev.* **52** 299–317
[8] Griessen R and Riesterer T 1992 *Hydrogen in Intermetallic Compounds* vol I ed L Schlapbach (Berlin: Springer) pp 219–84
[9] Springer T 1978 *Hydrogen in Metals* vol I ed G Alefeld and J Volkl (Berlin: Springer) pp 75–100
[10] Ross D K, Martin P F, Oates W A and Khoda Bakhsh R 1979 *Z. Phys. Chem., N F* **114** 221–30
[11] Ikeda S and Watanabe N 1987 *J. Phys. Soc. Japan* **56** 565–76
[12] Udovic T J, Rush J J, Huang Q and Anderson I S 1997 *J. Alloys Compounds* **253/254** 241–7
[13] Ikeda S, Furusaka M, Fukunaga T and Taylor A D 1990 *J. Phys.: Condens. Matter* **2** 4675–84
[14] Sugimoto H and Fukai Y 1979 *Phys. Rev.* B **22** 670–80
[15] Sugimoto H and Fukai Y 1981 *J. Phys. Soc. Japan* **50** 3709–17
[16] Sugimoto H and Fukai Y 1982 *J. Phys. Soc. Japan* **51** 2554–61
[17] Bennington S M and Ross D K 1993 *Z. Phys. Chem.* **181** 527
[18] Elsasser C, Ho K M, Chan C T and Fahnle M 1992 *J. Phys.: Condens. Matter* **4** 5207
[19] Ross D K, Antonov V E, Bokhenkov E L, Kolesnikov A I, Ponyatovsky E G and Tomkinson J 1998 *Phys. Rev.* B **58**
[20] Fukai Y and Sugimoto H 1981 *J. Phys. F: Met. Phys.* **11** L137–9
[21] Stonadge P R 1993 *Ph D Thesis* Birmingham University
[22] Fernandez J F, Kemali M and Ross D K 1997 *J. Alloys Compounds* **253/254** 248–51
[23] Hempelmann R, Richter D, Hartmann O, Karlsson E and Wappling R 1989 *J. Chem. Phys.* **90** (3) 1935–49
[24] Hansen M 1958 *Constitution of Binary Alloys* (New York: McGraw-Hill) pp 565, 573
[25] Fernandez J F, Cuevas F, Alguero M and Sanchez C 1995 *J. Alloys Compounds* **231** 78–84
[26] Johnson J R and Reilly J J 1978 *Inorg. Chem.* **17** 3103–7
[27] Rodriguez-Carvajal J 1993 *Physica B* **192** 55
[28] Skripov A V and Belyaev M Yu 1993 *J. Phys.: Condens. Matter* **5** 4767–74
[29] Miron N F, Shcherbak V I, Bykov V N and Levdik V A 1971 *Sov. Phys.–Crystallogr.* **16** 266
[30] Lawson A C and Zachariasen W H 1972 *Phys. Lett.* A **38** 1
[31] Irvine S J C, Ross D K, Harris I R and Browne J D 1984 *J. Phys. F: Met. Phys.* **14** 2881–97
[32] Fruchart D, Rouault A, Shoemaker C B and Shoemaker D P 1980 *J. Less-Common Met.* **73** 363–68
[33] Torrens I M 1972 *Interatomic Potentials* (New York: Academic)
[34] Fernandez J F, Ross D K, Kemali M and Sanchez C 1988 *Proc. Metal–Hydrogen Systems. Fundamentals and Applications* at press
[35] Didisheim J J, Yvon K, Fischer P and Shaltiel D 1980 *J. Less-Common Met.* **73** 355–62
[36] Didisheim J J, Yvon K, Shaltiel D, Fischer P, Bujard P and Walker E 1979 *Solid State Commun.* **32** 1087–90
[37] Irodova A V, Lavrova O A, Laskova G V and Padurets L N 1982 *Sov. Phys.–Solid State* **24** 22–7
[38] Fischer P, Fauth F, Skripov A V, Podlesnyak A A, Padurets L N, Zshilov A L and Ouladdiaf B 1997 *J. Alloys Compounds* **253/254** 282–5
[39] Friedel J 1972 *Ber. Bunsenges. Phys. Chemie.* **76** 828–31
[40] Vineyard G H 1957 *J. Phys. Chem. Solid* **3** 121–7
[41] Katz L, Guinan M and Borg R J 1971 *Phys. Rev.* B **4** 330–41
[42] Le Claire D 1966 *Phil. Mag.* **14** 1271–84
[43] Majer G, Renz W, Seeger A, Barnes R G, Shinar J and Skripov A V 1995 *J. Alloys Compounds* **231** 220–5
[44] Bowman R C, Craft B D Jr, Attalla A and Johnson J R 1983 *Int. J. Hydrogen Energy* **8** 801–8
[45] Renz W, Majer G, Skripov A V and Seeger A 1994 *J. Phys.: Condens. Matter* **6** 6367–74